



**Cross-Seeding Enables Repurposing of Aurein Antimicrobial Peptide as a Promoter of Human Islet Amyloid Polypeptide (hIAPP)**

Journal:	<i>Journal of Materials Chemistry B</i>
Manuscript ID	TB-ART-05-2023-001099.R1
Article Type:	Paper
Date Submitted by the Author:	17-Jun-2023
Complete List of Authors:	Tang, Yijing; University of Akron, Chemical and Biomolecular Engineering Zhang, Dong; University of Akron, Chemical and Biomolecular Engineering Gong, Xiong; University of Akron, Polymer Eng Zheng, Jie; University of Akron, Chemical and Biomolecular Engineering

**Cross-Seeding Enables Repurposing of Aurein Antimicrobial Peptide as a Promoter of Human Islet Amyloid Polypeptide (hIAPP)**

Yijing Tang<sup>1</sup>, Dong Zhang<sup>1</sup>, Xiong Gong<sup>2</sup>, and Jie Zheng<sup>1\*</sup>

<sup>1</sup>Department of Chemical, Biomolecular, and Corrosion Engineering  
The University of Akron, Ohio, USA

<sup>2</sup>School of Polymer Science and Polymer Engineering  
The University of Akron, Ohio, USA

\* Corresponding author: [zhengj@uakron.edu](mailto:zhengj@uakron.edu)

### Abstract

Since hIAPP (human islet amyloid polypeptide) aggregation and microbial infection are recognized as significant risk factors that contribute to the pathogenesis of type II diabetes (T2D), targeting these catastrophic processes simultaneously may have a greater impact on the prevention and treatment of T2D. Different from the well-studied hIAPP inhibitors, here we proposed and demonstrated a repurposing strategy for an antimicrobial peptide, aurein, which can simultaneously modulate hIAPP aggregation and inhibit microbial infection. Collective data from protein, cell, and bacteria assays revealed such dual functions of aurein including (i) promotion of hIAPP aggregation at a low molar ratio of aurein:hIAPP=0.5:1-2:1, (ii) reduction of hIAPP-induced cytotoxicity in RIN-m5F cells, and (iii) preservation of original antimicrobial activity against *E.coli.*, *S.A.*, and *S.E.* strains in the presence of hIAPP. Dual functions of aurein are mainly derived from its strong binding to different hIAPP seeds through conformationally similar  $\beta$ -sheet association. Our study provides a promising avenue for the repurposing of antimicrobial peptides (such as aurein) as amyloid modulators for blocking at least two pathological pathways in T2D.

## 1. Introduction

Type II diabetes (T2D) is a chronic metabolic disorder that is characterized by elevated levels of glucose in the blood (i.e., hyperglycemia), due to strong insulin resistance and/or insufficient insulin production in T2D patients<sup>1-4</sup>. As a multifaceted disease, risk factors for T2D include genetic predisposition, obesity, physical inactivity, high blood pressure, high cholesterol levels, and age<sup>5-9</sup>. From a perspective of pathogenic protein, human islet amyloid polypeptide (hIAPP, also known as amylin, **Fig. 1a**) is a hormone that produced and co-secreted with insulin by pancreatic  $\beta$ -cells in response to food intake<sup>10,11</sup>. In healthy individuals, hIAPP works with insulin to regulate glucose levels in blood by slowing down the rate at which food is absorbed from digestive tracts after meals. Moreover, hIAPP is known to regulate food intake by controlling appetite and satiety<sup>12,13</sup>. However, in people with T2D, hIAPP is often overproduced and aggregates into  $\beta$ -structure-rich amyloid fibrils in the pancreatic islets<sup>14</sup>. These hIAPP aggregates can damage pancreatic  $\beta$ -cells, leading to the progressive loss of insulin secretion and worsening of hyperglycemia, which are pathological hallmarks of T2D<sup>1,2</sup>.

Some drugs, such as pramlintide<sup>15</sup> (only FDA-approved drug), brazilin<sup>16</sup>, tanshinones<sup>17</sup>, aromadendrin<sup>18</sup>, metal ions<sup>19</sup> ( $\text{Hg}^{2+}$  and  $\text{Cd}^{2+}$ ), and polyphenols<sup>20-24</sup> (EGCG, resveratrol, curcumin) that modulate hIAPP aggregation have shown promise in improving  $\beta$ -cell function and glucose control in individuals with T2D. However, these drugs, which specifically target hIAPP aggregation, have shown limited effectiveness in treating T2D, due to several reasons<sup>23</sup>. Firstly, hIAPP aggregation is only one of several risk factors that contribute to the pathogenesis of T2D. Other factors such as insulin resistance,  $\beta$ -cell dysfunction, chronic inflammation, and metabolic dysregulation<sup>25-29</sup> also significantly impact the development and progression of T2D. Thus, drugs that solely target hIAPP aggregation may not be sufficient to address the multifaceted nature of the disease. Secondly, the mechanisms underlying hIAPP aggregation are complex and not fully understood<sup>30,31</sup>, making it challenging to develop drugs that can effectively inhibit the formation of amyloid fibrils without affecting normal hIAPP function or causing adverse effects. Moreover, these drugs often require high doses or prolonged treatment, leading to potential toxicity and adverse effects<sup>32</sup>.

Accumulating evidence suggests a triangular relationship between hIAPP aggregation, microbial infection, and T2D. Firstly, studies have shown that certain types of bacterial infections, such as periodontitis and gut infections, are more common in people with T2D<sup>33-35</sup>. Inflammation ( $\text{TNF-}\alpha$ ,  $\text{IL-1}\beta$ ,  $\text{IFN-}\gamma$ ) triggered by these microbial infections may interfere with insulin signaling pathways and impair glucose uptake by cells, leading to insulin resistance<sup>36,37</sup>, a typical hallmark of T2D. Also, an imbalance in the gut microbiome (known as dysbiosis) has been linked to insulin resistance and glucose intolerance<sup>38,39</sup>, both of which are associated with T2D. Secondly, viral infection by cytomegalovirus (CMV) and hepatitis C virus (HCV) can also trigger inflammation and interfere with insulin production and uptake<sup>40,41</sup>, which have been associated with an increased risk of developing T2D.

More importantly, in addition to microbial and viral infections, recent studies have suggested a potential link between hIAPP aggregation and microbial infections in T2D. hIAPP has been shown to stimulate cytokine production and enhance macrophage phagocytic activity, which promote the recruitment of immune cells in response to bacterial infections<sup>42,43</sup>. Conversely, microbial infection has been found to trigger hIAPP aggregation in pancreatic islet cells and exacerbate  $\beta$ -cell dysfunction<sup>44</sup>, thereby contributing to T2D pathogenesis. While the exact relationship between hIAPP aggregation and microbial infection in T2D is still not fully understood, targeting both hIAPP aggregation and microbial infection could be a more effective strategy for preventing and treating T2D than those single-target strategies.

Conceptually, a promising strategy for achieving both antimicrobial and anti-amyloid functions is to repurpose or discover antibacterial peptides with dual capacities of inhibiting amyloid formation as a new function and maintaining their intrinsic ability to combat microbial infections. Aurein1.2 (namely Aurein) is a naturally occurring antimicrobial peptide (AMP) that is isolated from the skin secretions of the Australian green tree frog (also known as *Litoria aurea*). Aurein is a cationic peptide consisting of 13 amino acid residues, with a net charge of +1 at physiological pH (**Fig. 1a**). Aurein exhibits a broad-spectrum antimicrobial activity against bacteria, fungi, and viruses by disrupting the cell membranes of target microorganisms, leading to cell lysis and death. Interestingly, aurein has been found to form  $\beta$ -sheet-like conformation (aggregated strands) after interacting with the charged lipids (with a molar ratio of aurein : dDPPG = 1:1), along with the subsequent descending  $\alpha$ -helical amide I signals<sup>45</sup>. While targeting difference cells, both hIAPP and aurein can disrupt membrane integrity through mechanisms of pore formation and membrane lysis.

Considering that both hIAPP and aurein share some similarities in their (mis)folded  $\beta$ -sheet structures and the membrane disruption mechanisms, here we discovered a new biological function of aurein as an amyloid promotor, not as an amyloid inhibitor. Collective results showed that aurein was capable of cross-seeding with hIAPP to achieve its multiple functions, including (i) promotion of hIAPP aggregation by 102% at a molar ratio of hIAPP:aurein=1:2; (ii) interaction with earlier hIAPP species of monomers, oligomers, but not mature fibrils, to accelerate hIAPP aggregation; (iii) protection of RIN-m5F pancreatic cells from hIAPP-induced toxicity reduction by increasing cell viability by 10-29% and reducing cytotoxicity by 9-36%; and (iv) retaining of high antibacterial activity against three bacterial strains, both Gram-negative and Gram-positive types, all of which are involved in different pathological pathways towards the onset and progression of T2D. Aurein not only has intrinsic antimicrobial activity, but also exhibits an additional function of promoting amyloid formation by hIAPP by quickly bypassing toxic oligomers formed at the lag-growth stage to non- or less toxic fibrils and shortening the exposure time of tissues/cells to toxic aggregates. This dual antimicrobial and anti-amyloid activity makes aurein a promising therapeutic agent for the treatment of T2D by targeting both the pathological pathways induced by hIAPP aggregation and microbial infection. However, further (pre)clinical research is needed to assess the

efficacy and safety of aurein in animal models and clinical settings.

## 2. Results and Discussion

### 2.1. Promotion of Amyloid Aggregation by Cross-Seeding of Aurein with Monomeric hIAPP

Based on the common potential of aurein and hIAPP to self-assemble into similar  $\beta$ -sheet-rich aggregates, we proposed a “like-interacts-like” mechanism, where aurein is expected to interact strongly with hIAPP through conformationally similar  $\beta$ -structure association. Such interactions between aurein and hIAPP can in turn modulate hIAPP-hIAPP self-aggregation. To test this hypothesis, we first investigated the potential inhibition or promotion effect of aurein on hIAPP aggregation by co-incubating freshly prepared hIAPP with aurein at different molar ratios of 1:0.5-1:2 at 37°C for 40 h. As shown in **Fig. 1b**, pure aurein, as a control, did not generate a ThT signal even at a high concentration of 40  $\mu$ M. This result not only indicate that this concentration is insufficient to trigger the self-assembly of aurein, but also rules out the possibility of aurein interfering with ThT intensity. Pure hIAPP (20  $\mu$ M) as another control exhibited a typical sigmoidal growth curve characterized by a nucleation-polymerization aggregation mechanism. The aggregation process began with a lag phase within 7 hours, followed by a rapid growth phase until 25 hours with the aggregation rate of  $\sim 8.3$  h<sup>-1</sup> (as calculated at  $t_{1/2}=13.5$  h), reached a stable plateau with a ThT intensity of approximately 221 a.u.

For comparison, when freshly dissolved hIAPP monomers were co-incubated with Aurein at different molar ratios (ranging from 1:0.5 to 1:2), hIAPP aggregation kinetics showed a dose-dependent increase at all stages of aggregation. This was evidenced by several observations: (i) a decrease in lag time from 7 hours to 4 hours, (ii) a decrease in half time ( $t_{1/2}$ ) from 12.5 hours to 5.1 hours, (iii) an increase in aggregate rate during the growth phase from 12 h<sup>-1</sup> to 71 h<sup>-1</sup>, and (iv) a promotion of final ThT intensity at the equilibrium phase by 15% to 102% (**Fig. 1c**). Morphologically, AFM images of co-incubated aurein and hIAPP samples, obtained at different time points, were shown in **Fig. 1d & Fig. S1**. At first glance, both homo- and cross-seeding aggregation can form amyloid fibrils during 24 hours, but they exhibit different fibril formation kinetics. As controls, pure hIAPP aggregation (20  $\mu$ M) underwent morphological changes and growth, starting from a few spherical aggregates with an average height/length of 12/180 nm at 6 hours to long, dense fibrils with an average height/length of 21/1040 nm at 24 hours. However, co-incubation of hIAPP with aurein at hIAPP: aurein molar ratios of 1:1-1:2 resulted in a significant acceleration of the hIAPP aggregation process, as evidenced by the increased formation of more dense and abundant fibrils at every time point between 6 h and 24 h. At longer incubation times, the cross-seeding-induced promotion effect became more pronounced. Furthermore, in all cross-seeding samples at three different molar ratios, fibrils formed at 24 h covered nearly the entire scanning area with average heights ranging from 29 to 42 nm, in sharp contrast to the scattered thin hIAPP fibrils formed alone.

To gain a deeper understanding of the promotion effect induced by cross-seeding between hIAPP and aurein, we analyzed the secondary structural changes during the entire fibrillization process of hIAPP (20  $\mu\text{M}$ ) with and without aurein (20-40  $\mu\text{M}$ ) using circular dichroism (CD) spectroscopy (Fig. S2). Firstly, pure aurein (20-40  $\mu\text{M}$ ) was used as a control and was found to retain random coil structures during 24 h incubation (Fig. S3). For the hIAPP-aurein systems, at the beginning of aggregation ( $t=0$  h), both hIAPP alone and all hIAPP-aurein systems exhibited a single negative peak at  $\sim 198$  nm, indicating a predominant random coil structure. As the aggregation progressed to 6 h, the hIAPP-aurein systems showed a larger structural transition compared to pure hIAPP, as evidenced by the transition to a  $\beta$ -sheet-rich structure (indicated by the negative peak at  $\sim 215$  nm and positive peak at  $\sim 195$  nm). This suggests that a  $\beta$ -sheet structure formed with the assistance of aurein. At the end of the aggregation process (24 h), all the hIAPP samples, with and without aurein, exhibited a characteristic  $\beta$ -sheet structure. However, hIAPP-aurein systems at all molar ratios showed higher peak intensities than hIAPP alone. Quantitative analysis of the secondary structure contents in Fig. 1e revealed that upon co-incubation of aurein with hIAPP for 24 h, the random coil structure decreased from 55.0% to 39.6-47.5%, while the  $\beta$ -structure increased from 43.5% to 52.0-56.8%, as compared with pure hIAPP incubation. These results, along with ThT and AFM results, suggest that the amyloidosis promotion effect induced by aurein could be attributed to the cross-seeding interaction between hIAPP and aurein, which could act as an anchor to associate hIAPP and stabilize the  $\beta$ -hairpin structure, thus promoting hIAPP aggregation.

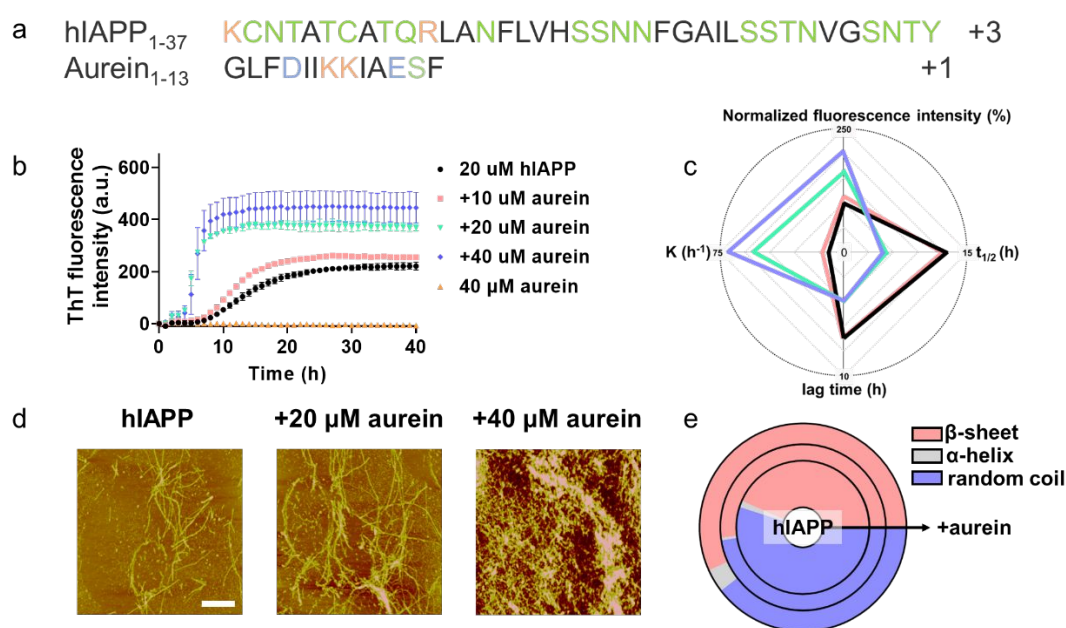


**Figure 1. Cross-seeding of aurein with hIAPP monomers promotes hIAPP aggregation.** (a) Sequence of hIAPP and aurein. Color ID: polar residues (green), non-polar residues (black), positively charged residues (orange), and negatively charged residues (blue). (b) Dose-dependent promotion effect of aurein (10-40  $\mu\text{M}$ ) on hIAPP (20  $\mu\text{M}$ ) aggregation by ThT fluorescence assays. Samples were prepared in ThT (10  $\mu\text{M}$ ) - Tris buffer solution (10 mM, pH=7.4) in 96-well plate at 37°C and recorded at every 1-hour interval. Data represent mean  $\pm$  standard error of triplicate measurements. (n=3). (c)

Analysis of hIAPP aggregation kinetics in the presence (colored) and absence (black) of aurein in terms of normalized ThT intensity, fibrillization rate, half time, and lag time. Final ThT fluorescence of pure hIAPP aggregation is used as a reference to define the relative ThT fluorescence ratio of hIAPP-aurein cross-seeding. (d) AFM images of pure hIAPP sample (20  $\mu\text{M}$ ) and cross-seeding hIAPP-aurein samples (1:1-1:2) after 24 h incubation. Scale bars are 1  $\mu\text{m}$ . Samples were prepared in PBS buffer (10 mM, pH=7.4) at 37°C. (e) Secondary structure distributions of hIAPP (20  $\mu\text{M}$ ) in presence of aurein of 0  $\mu\text{M}$  (inner cycle), 20  $\mu\text{M}$  (middle cycle), and 40  $\mu\text{M}$  (outer cycle), as analyzed by the BESTSEL program from circular dichroism (CD) spectra. Samples were prepared in PBS buffer (10 mM, pH=7.4) at 37°C.

## 2.2. Modulation of Amyloid Aggregation Pathways by Cross-seeding of Aurein with Different hIAPP Seeds

After demonstrating the cross-seeding of aurein with freshly prepared hIAPP monomers and the resultant promotion of hIAPP fibrilization, it is of greater interest to investigate whether aurein can also cross-seed with larger hIAPP species and, if so, how this cross-seeding may impact hIAPP fibrillization. To achieve this objective, we designed a novel seeding approach by the addition of aurein (40  $\mu\text{M}$ ) to distinct hIAPP seed solutions (20  $\mu\text{M}$ ) obtained from the 5 h lag, 11 h growth, and 23 h equilibrium stages. We subsequently assessed the effectiveness of cross-seeding by tracking changes in the aggregation kinetics (as measured by ThT signals, **Fig. 2a**) before and after adding aurein to hIAPP seed solutions. In **Fig. 2a**, addition of aurein (40  $\mu\text{M}$ ) to a preformed hIAPP seed solution obtained at 5 h resulted in an instantaneous and significant increase in ThT signal (red curve) compared to pure hIAPP. This growth process lasted for almost  $\sim 3$  h and finally reached a stable plateau of  $\sim 387$  a.u., which was 78% higher than that of pure hIAPP aggregation (black curve). Similarly, aurein-11h-seeded hIAPP system displayed almost the same ThT aggregation kinetics curve as aurein-5h-seeded hIAPP system. Upon adding aurein to the 11 h-seeded hIAPP solution, the ThT aggregation curve suddenly increased, followed by a quick approach to a stable plateau of  $\sim 387$  after 2 h growth time, showing 78% increase of final fibrils compared with pure hIAPP aggregation. These results indicate that aurein can interact efficiently with both hIAPP monomers and oligomers to accelerate their aggregation towards mature fibrils. However, the cross-seeding phenomenon nearly disappeared when adding aurein to the preformed hIAPP fibrils at 23 h, as indicated by the lack of growth rate increment and final fibril amounts in the ThT curve. ThT curves of aurein-23h-seeded hIAPP (green curve) and pure hIAPP (black curve) were almost overlapped, suggesting the absence of cross-seeding effect at this stage.

AFM and CD spectroscopy were used in parallel to confirm and understand the aurein-induced fibril promotion and structural transition of different hIAPP seeds. Pure hIAPP produced a few protofibrils with an average height/length of 21/1040 nm at 24 h as a control. Co-incubation of 40  $\mu\text{M}$  aurein with 5h- and 11h-hIAPP seeds led to obvious fibril acceleration, but in different extents, as visualized by longer and thicker mature fibrils with an average height/length of 24-46/ $\sim 2140$  nm (**Fig. 2c**). Aurein showed

inferior cross-seeding capacity with fibrillar hIAPP, as evidenced by a similar amount of fibril formation with an average height/length of 15/850 nm, consistent with ThT results in **Fig. 2a**. CD spectra showed that co-incubation of aurein (40  $\mu\text{M}$ ) with different hIAPP seeds led to the increase of the characteristic  $\beta$ -sheet-pertaining peak at 195 nm and 215 nm (**Fig. S4**). After 24 h incubation, the amount of  $\beta$ -sheets was increased by 7.6% (red line), 11.2% (blue line) and 2.1% (green line) for 5 h, 11 h, and 23 h hIAPP seeds, respectively (**Fig. 2b**).

Collective cross-seeding results showed that the efficiency of aurein in cross-seeding with different hIAPP seeds decreased in the following order: aurein-5h hIAPP seeds  $\approx$  aurein-11h hIAPP seeds  $>$  aurein-23h hIAPP seeds. This implies that aurein is more effective in promoting the aggregation and conversion of hIAPP formed in the early lag and growth phase, but less effective in transforming higher-ordered hIAPP species with more  $\beta$ -structure into  $\beta$ -structure-rich aggregates and catalyzing them into mature fibrils, indicating the presence of cross-seeding barriers. This may be due to (i) the higher conformational similarity and lower cross-species barrier between monomeric hIAPP and aurein, which share the same random coil structure, and (ii) the earlier hIAPP species having more unreacted binding sites for newly-added aurein to interact with, while older hIAPP species have most active sites occupied by hIAPP themselves. This conclusion was supported by AFM and CD spectroscopy results, which showed that co-incubation of aurein with different hIAPP seeds led to longer and thicker mature fibrils with increased  $\beta$ -sheet content, and that the increase in  $\beta$ -sheet content was greater for earlier hIAPP species than for older ones.

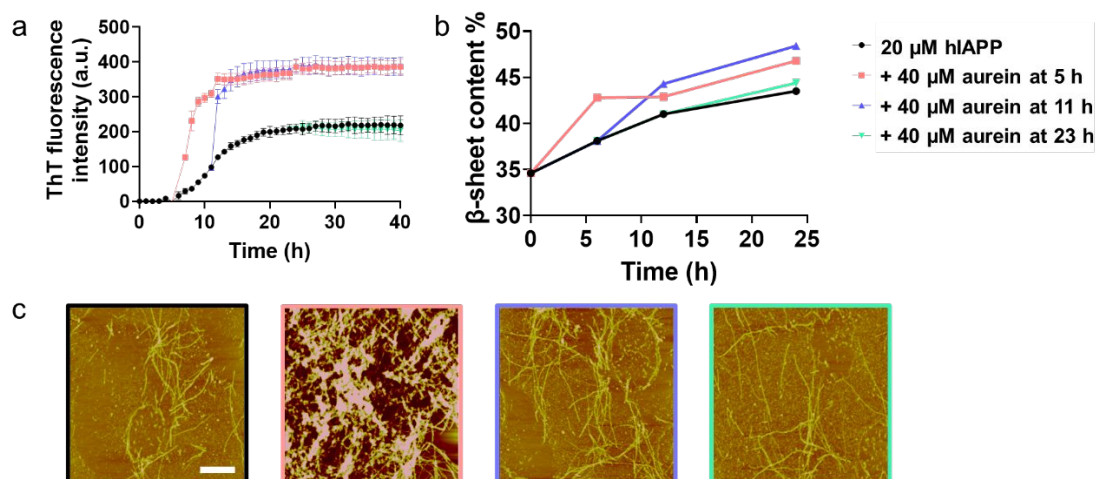


**Figure 2. Cross-seeding efficiency of aurein with different hIAPP seeds.** (a) Time-dependent ThT fluorescence curves showing the effect of aurein (40  $\mu\text{M}$ ) on hIAPP (20  $\mu\text{M}$ ) seeds preformed at the lag, growth, and equilibrium phases. Samples were prepared in ThT (10  $\mu\text{M}$ ) - Tris buffer solution (10 mM, pH=7.4) in 96-well plate at 37°C. Fluorescence readings were recorded at consistent 1-hour intervals. (b) CD spectra showing the  $\beta$ -sheet structure changes before and after adding aurein (40  $\mu\text{M}$ ) to hIAPP seeds (20  $\mu\text{M}$ ). Samples were prepared in PBS buffer (10 mM, pH=7.4) at 37°C. (c) Representative AFM images of the fibril morphology resulting from the addition of aurein (40  $\mu\text{M}$ ) to hIAPP seeds (20  $\mu\text{M}$ ) preformed at the 5 h-lag-phase (red), 11 h-growth-phase (blue), and 23 h-equilibrium-phase (green). Scale bars are 1  $\mu\text{m}$ . Samples were prepared in PBS buffer (10 mM, pH=7.4) at 37°C. The cross-seeding efficiency of aurein with different hIAPP seeds decreases in the order of aurein-5 h hIAPP seeds  $\approx$  aurein-11 h hIAPP seeds  $>$  aurein-23 h hIAPP seeds, indicating the existence of cross-seeding barriers.

### 2.3. Molecular Characterization of Binding Affinity of Aurein to Different hIAPP Seeds

From a molecular interaction viewpoint, the promotion of hIAPP fibrillation by aurein is mainly attributed to its cross-seeding with hIAPP and thereby modulate hIAPP-hIAPP self-interactions, leading to accelerated hIAPP fibrillation. To test this hypothesis, we used surface plasmon resonance (SPR) to measure the binding affinity between aurein and different hIAPP seeds, including freshly prepared monomers, 11-hour incubated oligomers, and 23-hour incubated fibrils. **Fig. 3a** illustrates the schematic workflow used to quantify the binding affinity between aurein and different hIAPP seeds (monomers, oligomers, and fibrils) using SPR. First, freshly prepared aurein was covalently immobilized on carboxymethylated dextran SPR chips via EDC/NHS coupling. Then, hIAPP seed solutions with concentrations ranging from 2.5-20  $\mu\text{M}$  were flowed over the immobilized aurein in the channels to determine the occurrence of specific binding between the two molecules (**Fig. 3b**). Upon initial observation, the SPR signals of aurein-coated surfaces showed immediate and dose-dependent responses to all hIAPP seeds, indicating specific binding between immobilized aurein and hIAPP seeds. The immobilized aurein absorbed more hIAPP monomers and oligomers than hIAPP fibrils at all concentrations tested (2.5, 5, 10, and 20  $\mu\text{M}$ ). Furthermore, the observation that the immobilized aurein absorbs more hIAPP seeds with increasing concentrations of hIAPP seeds suggests that there may be a concentration-dependent binding interaction between the aurein and hIAPP seeds.

To provide a more detailed analysis of the observation, the amount of hIAPP adsorbed on aurein-coated surfaces was measured at different concentrations. Specifically, as the concentration of hIAPP increased from 2.5 to 20  $\mu\text{M}$ , the adsorption amount of hIAPP on aurein-coated surfaces increased for all forms of hIAPP, i.e., from 38.8 to 233.4  $\text{ng}/\text{cm}^2$  for hIAPP monomers, from 34.9 to 275.9  $\text{ng}/\text{cm}^2$  for hIAPP oligomers, and from 18.7 to 58.1  $\text{ng}/\text{cm}^2$  for hIAPP fibrils. After washing with PBS buffer to remove any loosely bound hIAPP species, hIAPP monomers were found to have

a stronger binding affinity than hIAPP oligomers, as evidenced by the lower amount of hIAPP monomers washed off (i.e., 0-10.6 ng/cm<sup>2</sup> for hIAPP monomers vs. 0-37.9 ng/cm<sup>2</sup> for hIAPP oligomers). Further kinetic analysis revealed that hIAPP monomers and oligomers exhibited a lower dissociation constant ( $K_D$ ) of 2.83 and 5.15  $\mu$ M, respectively, which was 6 times and 3.3 times lower than the  $K_D$  of 17.14  $\mu$ M for hIAPP fibrils. These results suggest that aurein has a stronger binding affinity towards earlier hIAPP seeds compared to later fibrillar ones. Taken together, these findings suggest that immobilized aurein specifically binds to hIAPP seeds, with a higher affinity for earlier seeds such as monomers and oligomers, and a concentration-dependent binding interaction.

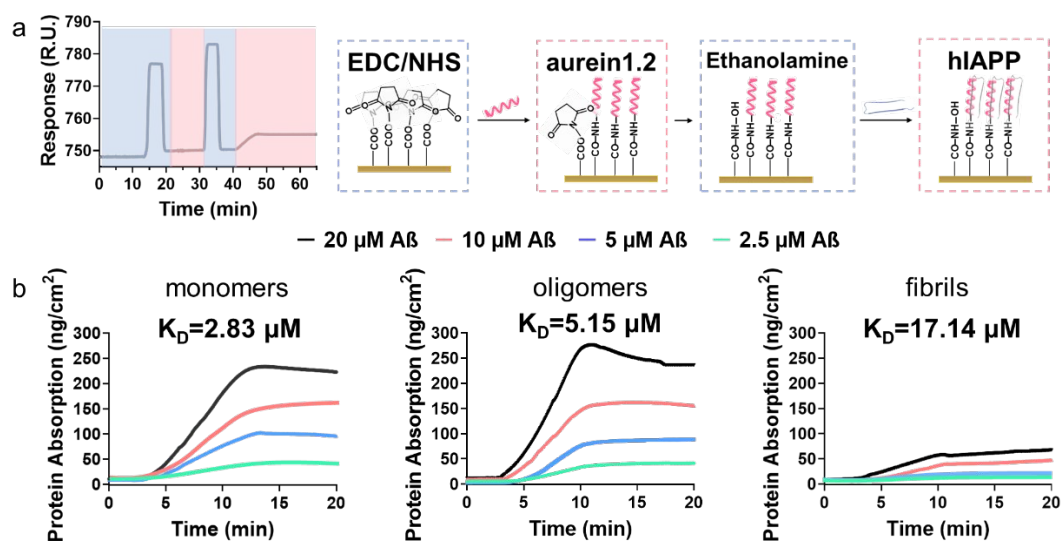


**Figure 3. Binding affinity of aurein to hIAPP aggregates of different concentrations and sizes by SPR.** (a) Schematic representation of the immobilization of aurein on the SPR chip for hIAPP binding. (b) SPR sensorgrams showing the adsorption amount of freshly prepared hIAPP (1<sup>st</sup> column), oligomeric hIAPP (2<sup>nd</sup> column), and fibrillar hIAPP (3<sup>rd</sup> column) at varied concentrations of 2.5-20  $\mu$ M on aurein-coated SPR surface. The adsorption amount of hIAPP aggregates was measured and analyzed to determine their binding affinity to aurein. hIAPP seeds were prepared in PBS buffer (10 mM, pH=7.4) at 37°C for different time periods, while aurein was freshly prepared.

#### 2.4. Rescue of Amyloid-Mediated Cytotoxicity by Cross-Seeding of Aurein with hIAPP

Amyloid oligomers are widely recognized as the main species responsible for causing cell death, as they are more toxic than amyloid fibrils. While many studies have focused on amyloid inhibitors to prevent aggregation and cytotoxicity<sup>46</sup>, aurein offers a unique property by promoting hIAPP fibrillization. This property allows aurein to potentially provide protection against hIAPP-induced cytotoxicity, as it rapidly converts toxic oligomers into less-toxic fibrils. To test this hypothesis, we investigated the cross-seeding effect of aurein with hIAPP on the RIN-m5F cell line using MTT to measure cell viability (**Fig. 4a**) and LDH assay to measure cell toxicity (**Fig. 4b**), where cell viability and toxicity data were normalized to an untreated cell control group (i.e., 100% cell

viability and 0% cytotoxicity). Pure aurein, as a control, exhibited no cytotoxicity on RIN-m5F cells, as demonstrated by 97%-99% cell viability and -0.6%-2.6% cytotoxicity during 24-hour cell culture. These results indicate that aurein at concentrations ranging from 10  $\mu\text{M}$  to 40  $\mu\text{M}$  is non-toxic to cells and does not affect their normal growth. In contrast, pure hIAPP at 20  $\mu\text{M}$  resulted in a 47% decrease in cell viability and a 46% increase in cell apoptosis after 24 hours of incubation, indicating the high toxicity of hIAPP aggregates to the cells. As compared to pure hIAPP, the co-incubation of aurein (10-40  $\mu\text{M}$ ) with hIAPP-treated cells led to a concentration-dependent increase in cell viability and decrease in cytotoxicity. Specifically, when introducing aurein into hIAPP-cultured cell solutions at a ratio of 1:0.5-1:2 for 24 hours, the resulting cell viability/cell apoptosis was 57%/37%, 64%/27%, and 76%/10%, which was 10%/9%, 17%/19%, and 29%/36% higher/lower than pure hIAPP-treated cells, respectively.

To visually demonstrate the protective effect of aurein from hIAPP-induced cell toxicity, we performed live/dead cell assay by staining live cells with Calcein AM (green) and dead cells with Ethidium homodimer-1 (red). Upon overlaying the green and red fluorescent images, **Fig. 4c** consistently showed that aurein alone did not exhibit any toxicity towards cells, with a large proportion of live cells (green stains) as compared to dead ones (red stains), similar to the control group. In contrast, hIAPP alone resulted in a significant number of dead cells (red stains) and a reduction in living cells. Co-incubation of aurein with hIAPP resulted in much fewer dead cells as compared to the pure hIAPP system, further confirming the protective ability of aurein against hIAPP-induced cell toxicity. Quantitatively, it is evident that the addition of aurein (40  $\mu\text{M}$ ) to A $\beta$  (20  $\mu\text{M}$ ) resulted in a significant 59.4 % reduction in the dead/live cell ratio.

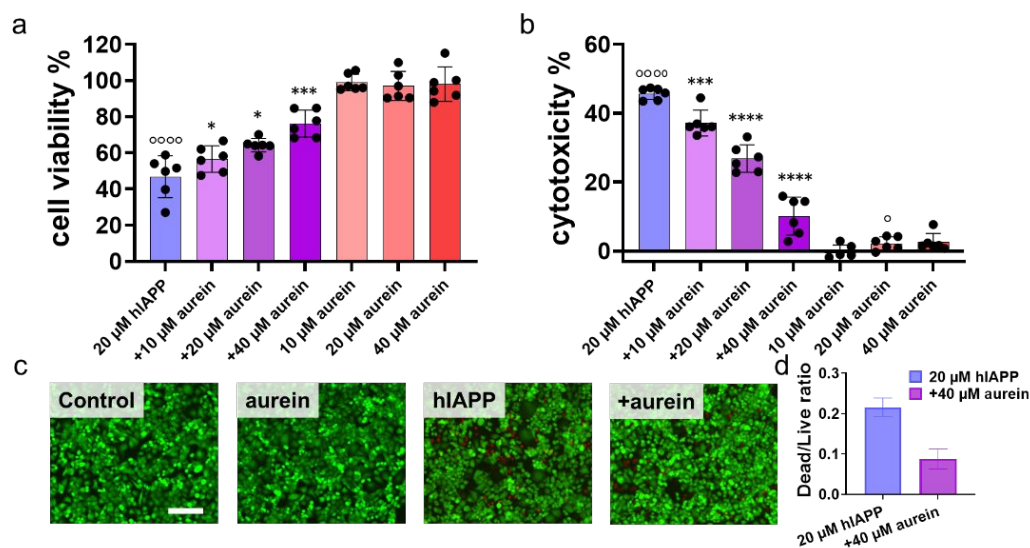


**Figure 4. Protection against amyloid-induced toxicity by cross-seeding of aurein with hIAPP.** (a) Cell viability by MTT assay and (b) cell cytotoxicity by LDH assay in RIN-m5F cells treated with hIAPP (20  $\mu\text{M}$ ) alone or co-incubated with aurein at molar ratios of 1:0.5, 1:1, and 1:2 for 24 h. Untreated cells were used as control (100% MTT reduction and 0% LDH activity), and cells treated with 10x Lysis Buffer were used as a

positive control for 100% LDH activity. Data represent mean  $\pm$  s.d. of three independent experiments. Statistical analysis ( $n = 3$ ) was performed for cells with both aurein and hIAPP compared to untreated cells ( $^{\circ}$ ,  $p < 0.05$ ;  $^{\circ\circ}$ ,  $p < 0.01$ ;  $^{\circ\circ\circ}$ ,  $p < 0.001$ ) or cells treated with hIAPP alone ( $*$ ,  $p < 0.05$ ;  $**$ ,  $p < 0.01$ ;  $***$ ,  $p < 0.001$ ). (c) Representative fluorescence microscopy images of live (green) and dead (red) RIN-m5F cells after 24 h of treatment with freshly prepared hIAPP (20  $\mu\text{M}$ ) in the absence or presence of 40  $\mu\text{M}$  aurein. Untreated cells were used as control. Scale bars represent 180  $\mu\text{m}$ . (d) Analysis of live/dead cell ratios for cells treated with freshly prepared hIAPP (20  $\mu\text{M}$ ) solutions co-incubated with and without aurein (40  $\mu\text{M}$ ) for 24 hours. RIN-m5F cells were cultured in 25  $\text{cm}^2$  T-flasks in sterile-filtered ATCC-formulated RPMI-1640 Medium containing 10% fetal bovine serum and 1% penicillin/streptomycin.

## 2.5. Cross-Seeding of Aurein with hIAPP Preserves Antimicrobial Properties

Considering that (i) aurein possesses an intrinsic antimicrobial property<sup>47</sup>; (ii) hIAPP has been recently recognized as an effective antimicrobial agent against clinically relevant bacteria<sup>48</sup>; (iii) amyloid and antimicrobial peptides share common mechanism of disrupting cell membranes to kill target cells; and (iv) both “amyloid cascade” and “microbial infection cascade” are linked to the pathogenesis of T2D, here we aimed to determine whether cross-seeding would enhance or weaken the antimicrobial capacity of aurein in the presence of hIAPP. To investigate the antimicrobial properties of aurein, hIAPP, and their heterocomplexes, we assessed their activity against Gram-negative bacterial strains including *Escherichia coli* (*E. coli.*) and *Pseudomonas aeruginosa* (*P.A.*) as well as Gram-positive bacterial strains including *Staphylococcus aureus* (*S.A.*) and *Staphylococcus epidermidis* (*S.E.*). As a control, aurein demonstrated broad-spectrum antibacterial activity against all four bacterial strains tested, albeit with varying efficiencies. Gram-positive bacteria are more susceptible to aurein (1-80  $\mu\text{M}$ ) due to the lack of an outer membrane, resulting in overall higher antimicrobial activity against *S.E.*, *S.A.*, *E. coli.*, and *P.A.* in descending order of antibacterial efficacy (**Fig. S6**). These findings are consistent with previous studies on the antimicrobial activity of aurein. Specifically, 80  $\mu\text{M}$  of aurein completely inhibited the growth of *S.A.* and *S.E.*, but it showed lower antimicrobial activity against *E. coli* and *P.A.* at the same concentration, with higher bacteria viability of 26% and 78%, respectively, over the same incubation period. Since *P.A.* was not highly susceptible to aurein, it was not included in subsequent tests.

To quantitatively evaluate the antibacterial potency of aurein and hIAPP in combination, a checkerboard assay was performed. The MICs of pure hIAPP (1<sup>st</sup> column) and pure aurein (1<sup>st</sup> row) were first analyzed and served as controls with the lowest concentrations (i.e.,  $\text{OD}_{600}=0.1$ ) to evaluate the combined effect of hIAPP and aurein. The checkerboard color map in **Fig. 5a-c** revealed that pure aurein exhibited complete inhibition (i.e., dark blue,  $\text{OD}_{600} < 0.1$ ) against all three types of bacterial strains as concentrations increased from 0 to 80  $\mu\text{M}$ . In contrast, pure hIAPP showed inferior antibacterial activity, with the lowest  $\text{OD}_{600}$  of 0.29 for *S.A.*, 0.26 for *S.E.*, and 0.28 for *E. coli.*, respectively. Quantitatively, aurein exhibited a higher antibacterial activity with

lower MIC values (20  $\mu\text{M}$  for *S.A.*, 20  $\mu\text{M}$  for *S.E.*, and 10  $\mu\text{M}$  for *E. coli.*), as compared to hIAPP (MIC > 80  $\mu\text{M}$  for all bacteria strains). When hIAPP-aurein heterocomplexes were co-incubated with bacteria, the combination (purple box in **Fig. 5a-c**) showed FIC indexes of 0.5-1.5, indicating no or slight improvement in inhibitory activity compared to the sum of individual FIC values of aurein and hIAPP (**Fig. 5d**). This suggests that the combination did not significantly enhance the antimicrobial properties of either aurein and hIAPP peptide.

To better understand the impact of cross-seeding between aurein and hIAPP on bacterial strains, we utilized a live/dead staining assay to monitor the bacterial membrane integrity and distinguish between live (green) and dead (red) bacteria in the presence of aurein and hIAPP. A representative hIAPP-aurein combination (indicated by the purple box in **Fig. 5a-c**) and corresponding pure hIAPP (blue box in **Fig. 5a-c**) or aurein (red box in **Fig. 5a-c**) were selected at the FIC point for further analysis using the live/dead staining assay. As shown in the control groups (grey boxes) in **Fig. 5e-g**, all bacterial strains exhibited massive green fluorescence indicating normal bacterial growth without any treatment. In contrast, all samples treated with pure aurein (red box) or hIAPP (blue box) showed significant antimicrobial activity as evidenced by decreased bacterial density (i.e., less fluorescence signal) and a lower ratio of live (green) to dead (red) bacteria, confirming the antibacterial properties of pure aurein and hIAPP. When bacterial strains were co-incubated with hIAPP-aurein complexes, the bacterial density was further reduced compared to the treatment with pure aurein or hIAPP alone, as indicated by the almost no observable fluorescence signal. This reduction in bacterial density confirms the anti-bacterial growth capacity of the hIAPP-aurein complexes, suggesting that the assemblies still retain or even improve the bacterial killing property.

In parallel, the growth curves of the bacterial strains in **Fig. 5h-j** showed that the control groups of *S.A.*, *S.E.*, and *E. coli.* exhibited typical sigmoidal growth curves, each starting with a short lag phase of 0.5-2 h, followed by a rapid growth phase of 6.5-9.5 h, and finally reaching a saturated phase with the OD<sub>600</sub> values of 0.88, 0.97, and 0.70, respectively. In comparison, pure aurein and hIAPP showed significant antibacterial activity through one or more pathways: (i) prolonging the lag phase (e.g., *S.E.* and *E. coli.*); (ii) slowing down the growth rate (e.g., *S.E.*); and (iii) reducing the final bacterial density (e.g., *S.A.*, *S.E.*, and *E. coli.*). This suggests that they are effective in inhibiting bacterial growth. Quantitatively, both pure aurein and hIAPP showed significant reduction in bacteria density, with decreases in OD<sub>600</sub> values of 4.8% and 35% for *S.A.*, 79% and 53% for *S.E.*, and 15% and 27% for *E. coli.*, respectively. In the case of co-assemblies-treated systems, hIAPP-aurein heterocomplexes retained or even improved their antimicrobial activities compared to their pure forms. Specifically, co-incubation of aurein and hIAPP with *S.A.*, *S.E.*, and *E. coli.* strains resulted in significant enhancements in antimicrobial activity by 95.2%, 3%, and 52% as compared to pure aurein, as well as by 65%, 29%, and 40% as compared to pure hIAPP.

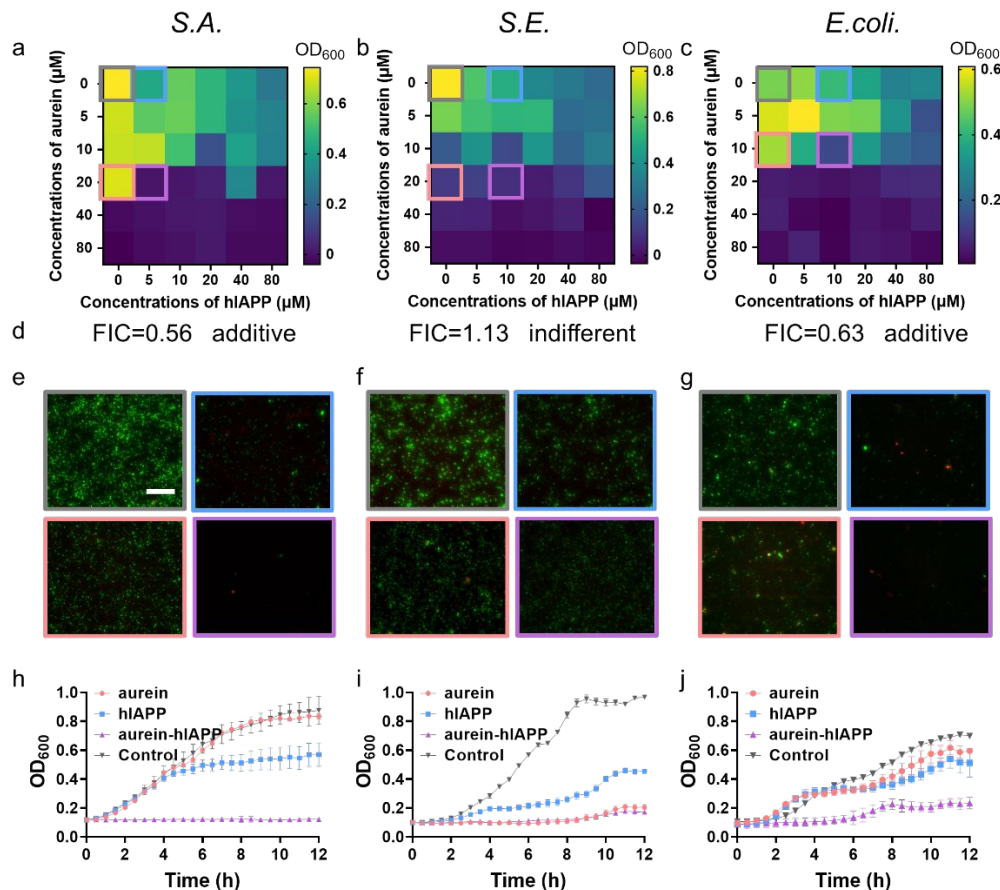


**Figure 5. hIAPP-aurein complexes retain a broad-spectrum antimicrobial property.**

(a-c) Checkerboard assay to determine the antibacterial potency of aurein (0-80  $\mu\text{M}$ ), hIAPP (0-80  $\mu\text{M}$ ), and their combination against Gram-positive (a) *S. A.*, (b) *S. E.*, and Gram-negative (c) *E. coli*. Wells with bacteria showing no growth are indicated by  $OD_{600}$  values of  $<0.1$  after 24 h growth. (d) Fractional inhibitory concentration (FIC) index of the combination of aurein and hIAPP (purple box) as calculated from the checkerboard assay. Synergy ( $\text{FIC} \leq 0.5$ ), additive ( $0.5 < \text{FIC} \leq 1$ ), indifferent ( $1 < \text{FIC} \leq 4$ ), and antagonism ( $\text{FIC} > 4$ ). **Growth profiles of (e) *S. A.*, (f) *S. E.*, and (g) *E. coli*. cultured in the absence (control, grey) and presence of pure aurein, pure hIAPP, and aurein-hIAPP heterocomplexes at FIC point. All data are represented as mean  $\pm$  standard error of triplicate measurements. (h-j) Representative fluorescence microscopy images of cells treated with freshly prepared hIAPP in the absence or presence of aurein at the FIC point. Untreated cells were used as a control. Red and green fluorescence indicate dead and live cells, respectively. The scale bars in live/dead images are 180  $\mu\text{M}$ . *E. coli* and *S. E.* were cultured in Difco™ LB Broth while *P. A.* and *S. A.* were cultured in BBL™ Trypticase™ Soy broth overnight at 37 °C, with the shaking speed of 120 rpm. Bacteria were further diluted to an  $OD_{600}$  value of 0.05, which is ready to use.**

### 3. Conclusions

Given that both hIAPP aggregation and microbial infection are both important factors in the pathogenesis of T2D, developing new therapeutic strategies and drugs that can simultaneously target both catastrophic processes may provide new and more

effective avenues for the prevention and treatment of T2D. Different from the well-studied hIAPP inhibitor, here, we discovered a new biological function of antimicrobial aurein as a promotor to modulate hIAPP aggregation and against hIAPP-induced cytotoxicity. As a promotor of hIAPP aggregation, our collective aggregation data from ThT, CD, and AFM experiments showed that aurein can cross-interact with different forms of hIAPP seeds, including monomers and oligomers, but not fibrils, to promote hIAPP aggregation through multiple pathways. These data suggest that aurein has a broad-spectrum promotion effect on hIAPP aggregation and can target different stages of the aggregation process. The ability of aurein to promote hIAPP aggregation through multiple pathways may be attributed to its strong binding affinity to hIAPP seeds via conformationally similar  $\beta$ -sheet association, as demonstrated by high binding affinity of  $K_D=2.83-17.14 \mu\text{M}$  from SPR assays. Furthermore, MTT and live/dead cell assays showed that aurein treatment increased cell viability by 10-29% and reduced cytotoxicity by 9-36%, indicating that aurein can rescue RIN-m5F cells from hIAPP-induced cytotoxicity by quickly bypassing toxic oligomer to fibril. Finally, despite cross-seeding with hIAPP, aurein maintained its antibacterial activity, which was comparable or even superior to that of pure aurein when tested against three types of Gram-positive and Gram-negative bacteria. It is worthy to note that we have also performed experiments specifically aimed at examining the potential impact of aurein 1.2 on the aggregation and toxicity of A $\beta$ . However, as shown in the **Fig. S7**, our findings from ThT data indicated that varying concentrations of aurein 1.2 (ranging from 5-40  $\mu\text{M}$ ) had minimal to no discernible effect on the aggregation of A $\beta$  (20  $\mu\text{M}$ ). These results suggest that aurein 1.2 exhibits a sequence-dependent interaction effect with distinct amyloid proteins.

This discovery suggests that aurein may have promising therapeutic potential for the treatment of T2D, because aurein has been shown to alleviate hIAPP-induced cytotoxicity and treat microbial infections simultaneously, where both hIAPP aggregation and microbial infections are involved in the onset and progression of T2D. More importantly, compared with hIAPP inhibitors which will simultaneously cut off the normal biological functions of hIAPP as a hormone, hIAPP promoter seems to be less worried. Further research is needed to test the efficiency and safety of aurein in animal models and clinical trials related to T2D. While aurein possesses antimicrobial, anticancer, and anti-hIAPP properties, the potential use of aurein to develop drugs has some limitations that need to be considered. These include: (i) Selectivity: It is important to determine if aurein selectively targets specific biological processes and avoids off-target effects; (ii) Toxicity: Assessing the safety profile and potential adverse effects of aurein is necessary; (iii) Pharmacokinetics: Understanding how aurein is metabolized and distributed in the body is crucial for its efficacy as a drug; (iv) Formulation and delivery: Developing a suitable formulation and delivery system for aurein is essential for its effective administration. Thus, while aurein shows promise in interfering with amylin, its selectivity, toxicity, pharmacokinetics, formulation, and regulatory considerations need to be thoroughly evaluated before considering its broader use as a therapeutic agent<sup>23,49,50</sup>.

## Experimental Procedures

### Reagents

Human islet amyloid polypeptide (hIAPP<sub>1-37</sub>,  $\geq 95\%$ ) and aurein ( $\geq 98\%$ ) was purchased from CPC Scientific (Sunnyvale, CA). 1,1,1,3,3,3-hexafluoro-2-propanol (HFIP,  $\geq 99.9\%$ ), dimethyl sulfoxide (DMSO,  $\geq 99.9\%$ ), and thioflavin T (ThT, 98%) were commercially available from Sigma Aldrich (St. Louis, MO). All other chemicals were of the highest grade available.

### Peptide Purification and Preparation

All the peptides were stored at  $-20\text{ }^{\circ}\text{C}$  immediately once arrived. To break any possible preformed amyloid aggregates, all the pre-packaged peptides (i.e., hIAPP and aurein) were re-dissolved in HFIP at the concentration of  $1\text{ mg/mL}$  and incubated at the ambient temperature for 2 h, followed by 30 min sonication in ice bath, 30 min centrifugation at 14000 rpm and  $4\text{ }^{\circ}\text{C}$  and sub-packaged according to experiment needs. Unless otherwise states, all peptides were freeze-dried for 1 h to remove all the HFIP and dissolved in different buffers ( $10\%$   $10\text{ mM NaOH}$ ) to reach desired concentration.

### Thioflavin T (ThT) Fluorescence Assay

Amyloidosis kinetics of hIAPP were recorded consistently at 30 min intervals by using SpectraMax M3 microplate reader (Molecular Devices, CA, USA) and measured at excitation wavelength of 450 nm and emission wavelength at the range of 470 nm to 500 nm under kinetic top-read mode. The ThT stock solution was prepared by dissolving ThT powder in Milli-Q water at the concentrations of  $2\text{ mM}$  and stored in dark place at room temperature. The stock solution was then sonicated to particle-free state and diluted in Tris buffer to  $10\text{ }\mu\text{M}$  before use. Samples were then prepared on ice by dissolving freeze-dried hIAPP in ThT ( $10\text{ }\mu\text{M}$ ) - Tris buffer solution ( $10\text{ mM}$ ,  $\text{pH}=7.4$ ) with and without  $10\text{-}40\text{ }\mu\text{M}$  aurein. For seeding experiment,  $5\text{ }\mu\text{L}$  aurein-NaOH mixture were added into aggregating hIAPP solution at 5, 11, and 23 h and kept monitor aggregation curves to illustrate the cross-seeding between aurein and hIAPP seeds.

### Circular Dichroism Spectroscopy (CD)

The secondary structures of hIAPP were examined by far-UV CD spectroscopy with a J-1500 spectropolarimeter (Jasco Inc., Japan) using a continuous scanning mode at room temperature. Samples were prepared on ice by dissolving freeze-dried hIAPP in PBS buffer ( $10\text{ mM}$ ,  $\text{pH}=7.4$ ) with and without  $10\text{-}40\text{ }\mu\text{M}$  aurein. For seeding experiment,  $15\text{ }\mu\text{L}$  aurein-NaOH mixture were added into pre-incubated hIAPP solution for 5, 11, and 23 h. To obtain the CD spectrum,  $150\text{ }\mu\text{L}$  of samples were pipetted into a  $1\text{ mm}$  optical path length CD cuvette and the spectra of the solution samples were recorded between  $190\text{-}250\text{ nm}$  at  $0.5\text{ nm}$  resolution and  $50\text{ nm/min}$  scan rate. all spectra were analyzed by subtracting the PBS buffer baseline to remove the background signal. The secondary structural contents were determined by using the Beta Structure Selection (BeStSel) algorithm<sup>51</sup> (<http://bestsel.elte.hu/>).

### Atomic Force Microscopy (AFM)

The tapping-mode AFM was employed to study the morphological changes of hIAPP aggregation mediated by aurein. To consistent with the conformational changes, 10  $\mu\text{L}$  sample solution from CD experiment was deposited on a piece of cleaved mica for 5 min, followed by 3x rinsing with Mill-Q water to totally remove additional salt and drying with an air stream before stored in a sealed container. All images were recorded at the  $256 \times 256$  pixel resolution at a typical scan rate of 1.0-2.0 Hz and with the vertical tip oscillation frequency of 250-350 kHz. For each sample, the representative AFM images were obtained by scanning six different locations on the mica surface. Depth data is acquired by using the Nanoscope analysis software and length data was calculated from all the fibrils shown in AFM images (up to  $N=40$ ).

### Surface Plasmon Resonance (SPR) Spectroscopy

The binding preference analysis was performed using a custom-built four-channel SPR instrument at ambient temperature. A dextran-modified SPR sensor chip was prepared following the well-established method<sup>52</sup>. Briefly, the clean gold surface was first immersed in a 5 mM 11-mercapto-1-undecanol in ethanol/water (8:2) solution for 24 h to obtain the thiol-based surface, followed by reacting with epichlorohydrin (2% v/v) in 0.1 M NaOH for 3 h and transferred to a 300 g/L dextran solution (500 kDa) in 0.1 M NaOH for 24 h to obtain the carboxymethylated dextran modified SPR chips. The resultant surfaces were finally washed with Milli-Q water and subsequently immersed in 1.0 M bromoacetic acid in 2 M NaOH for 24 h to achieve the dextran-modified SPR sensor chip.

For aurein immobilization, the PBS buffer was first injected to flow through four separated channels under the pressure of a peristaltic pump for 10 min to get the baseline. the SPR chips were then activated by an equimolar mixture of NHS (N-hydroxysuccinimide) and EDC (N-ethyl-N-(diethylaminopropyl) carbodiimide). Subsequently, aurein dissolved in PBS (10 mM, pH=7.4) were introduced to the sample surface for 10 min. To end the amine coupling reaction, 1 M ethanolamine HCL (pH=8.5) was injected for another 10 min. The binding affinity of aurein with hIAPP was performed by injecting a serial diluted hIAPP (2.5-20  $\mu\text{M}$ ) in running buffer (10 mM PBS, pH=7.4) over channels at a flow rate of 5  $\mu\text{L}/\text{min}$ , followed by PBS buffer to remove any unbounded amyloid peptides. In this work, 1nm of the SPR wavelength shift at 750 nm represents a surface coverage of  $\sim 15 \text{ ng}/\text{cm}^2$  protein absorption. Dissociation constant ( $K_D$ ) values were evaluated using Anabel software (<http://anabel.skscience.org/>) by fitting the data using a 1:1 Langmuir binding model and observed binding constant (kobs) linearization method.

### Cell Culture

Rat insulinoma cells RIN-m5F (ATCC® CRL-11605™, Manassas, VA) was used as in-vitro cell model to study the protection capacity of aurein on hIAPP-induced cytotoxicity. Cells were cultured in 25  $\text{cm}^2$  T-flasks in sterile-filtered ATCC-formulated RPMI-1640 Medium (ATCC, Manassas, VA) containing 10% fetal bovine serum (ATCC, Manassas,

VA) and 1% penicillin/streptomycin (ATCC, Manassas, VA). Flasks were incubated in a humidified incubator with 5% CO<sub>2</sub> at 37°C. Cells were then cultured to ~80% confluence and harvested using 0.25% Trypsin-EDTA (1x) solution (Lonza, Walkersville, MD) and seeded in 96-well plate (2×10<sup>5</sup> per well).

### Cell Assays

A colorimetric 3-(4,5-dimethylthiazole-2-yl)-2,5-diphenyltetrazolium bromide (MTT) metabolic activity assay and lactate dehydrogenase (LDH) assay was used to determine cell viability and cytotoxicity, respectively. RIN-m5F cells were allowed 24 h to grow and attach the bottom surface after seeding in 96-well plate. The media was then replaced with fresh media containing hIAPP (20 μM), aurein (10-40 μM), and hIAPP-aurein, which was further incubated for 24 h at 37 °C and 5% CO<sub>2</sub> in a humidified incubator. Subsequently, to the set up spontaneous/maximum LDH Activity and Maximum LDH activity controls, 10 μL of sterile, ultrapure water (as positive control) and 10X Lysis buffer (as negative control) was added to one set of triplicate wells of cells and incubated for 45 min, followed by transferring 50 μL of supernate medium from each well to a clean 96-well plate. Aliquot 50 μL of Reaction Mixture to each sample well, mix well and incubate for another 30 min. Finally, 50 μL of stop solution was added to each well and measure the absorbance at 490 nm and 680 nm by using SpectraMax M3 microplate reader. To determine LDH activity, subtract the 680-nm absorbance value (background) from the 490-nm absorbance before calculation of % cytotoxicity.

Calculate % Cytotoxicity by using the following formula:

$$\% \text{ cytotoxicity} = \left( \frac{\text{PG} - 1 \text{ treated LDH activity} - \text{spontaneous LDH activity}}{\text{maximum LDH activity} - \text{spontaneous LDH activity}} \right) \times 100\%$$

The old 96-well plate was used for MTT assay. In short, cells were labelled in 0.5 mg/mL MTT culture medium solution at 37 °C for 4 h and dissolved the formazan crystals in dimethyl sulfoxide. The absorbance value was read at 540 nm by using SpectraMax M3 microplate reader, and the cell viability was determined as the percentage of MTT reduction as compared to untreated cells. For both MTT and LDH, each sample was counted in triplicate and reported as mean ± SD.

The representative images of the live and dead cells were conducted using a LIVE/DEAD® Viability/Cytotoxicity Kit (L3224, Invitrogen) and imaged by fluorescence microscope (Echo RVL2-K) to visualize the live and dead cells. Corresponding fluorescence intensity was calculated by using Image J (n=3).

### Bacteria Culture

*Escherichia coli* (ATCC 8739), and *Staphylococcus epidermidis* (ATCC 14990) were cultured in Difco™ LB Broth (Sparks, MD) while *Pseudomonas aeruginosa* (ATCC 27853) and *Staphylococcus aureus* (ATCC 6538P) were cultured in BBL™ Trypticase™ Soy broth (Sparks, MD). All the bacteria strains were cultured overnight at 37 °C, 120 rpm and further diluted to an OD<sub>600</sub> value of 0.05, which is ready to use. For each well,

100  $\mu\text{L}$  bacterial solution was mixed with 1  $\mu\text{L}$  hIAPP, aurein, hIAPP-aurein dissolved in DMSO at desired concentration. As a control, an equal volume of DMSO was added correspondingly in control groups.

### Bacteria Assay

The growth curves of bacteria were then recorded by measuring the  $\text{OD}_{600}$  in the following 12 h at 30 min intervals at 37  $^{\circ}\text{C}$  by SpectraMax M3 microplate reader.

The representative images of the live and dead bacteria were acquired to evaluate the antibacterial effects of each hIAPP, aurein and their complexes. The Gram-negative *E. coli* bacteria and Gram-positive *S. aureus* bacteria incubated with or without peptides were stained using a LIVE/DEAD<sup>®</sup> BacLight<sup>™</sup> Bacterial Viability Kit (L7012, Invitrogen) and imaged by fluorescence microscope (Echo RVL2-K) to visualize the live and dead bacteria.

A checkerboard analysis is conducted to determine the antibacterial potency of the combination of hIAPP and aurein in comparison to their individual activities. To quantify the interactions between amyloid peptides and  $\alpha$ -defensins, the Fractional Inhibitory Concentration (FIC) index is introduced by the equation:

$$\frac{A}{\text{MIC}_A} + \frac{B}{\text{MIC}_B} = \text{FIC}_A + \text{FIC}_B = \text{FIC}_{\text{index}}$$

where A and B are the MIC of each peptide in combination, and  $\text{MIC}_A$  and  $\text{MIC}_B$  are the MIC of each peptide alone. The combining effect is interpreted as: synergy, FIC index  $\leq 0.5$ ; additive or indifference,  $0.5 < \text{FIC index} < 4.0$ ; antagonism, FIC index  $\geq 4.0$ .

In detail, in a 96-well plate, a serial dilutions of hIAPP (at concentrations from 0-80  $\mu\text{M}$ ) were added from columns 2 to 7, while a serial dilutions of aurein (at concentrations from 0-80  $\mu\text{M}$ ) were added from rows B to G. i.e., column 2 contains a serial dilution of hIAPP alone, while row B contains a serial dilution of aurein alone, which are set as controls to determine the MIC value for individual peptides alone. 100  $\mu\text{L}$  bacterial suspensions (initial  $\text{OD}_{600}=0.05$ ) with and with different combinations concentrations of hIAPP and aurein were added to each well and incubated at 37  $^{\circ}\text{C}$  for 24 h. The amount of growth in each well is quantified by  $\text{OD}_{600}$  and compared with that in the pure bacteria growth control. Wells with bacteria in no growth are determined by  $\text{OD}_{600} < 0.1$ .

### Declarations

- **Ethics approval and consent to participate:** Not applicable
- **Consent for publication:** Yes
- **Availability of data and materials:** All data are available in the main text or the supplementary materials.
- **Competing interests:** There is no competing interests.

- **Authors' contributions:** Y.T., J.Z., initiated the idea of this project. Y.T., D.Z. designed and conducted experiments in vitro. J.Z. supervised this project. The manuscript was written through the inputs of all the authors. All authors have given approval to the final version of the manuscript.
- **Acknowledgment.** We thank financial support from NSF-CBET-2107619. We also trained three high school students - Bowen Zheng from Copley High School, Alice Xu from Hudson High School, and Keven Gong from Western Reserve Academy – by this project.

## Reference

- (1) Selkoe, D. J. Folding proteins in fatal ways. *Nature* **2003**, *426* (6968), 900.
- (2) Lorenzo, A.; Razzaboni, B.; Weir, G. C.; Yankner, B. A. Pancreatic islet cell toxicity of amylin associated with type-2 diabetes mellitus. *Nature* **1994**, *368* (6473), 756.
- (3) Milardi, D.; Gazit, E.; Radford, S. E.; Xu, Y.; Gallardo, R. U.; Caflisch, A.; Westermark, G. T.; Westermark, P.; Rosa, C. L.; Ramamoorthy, A. J. C. R. Proteostasis of islet amyloid polypeptide: a molecular perspective of risk factors and protective strategies for type II diabetes. **2021**, *121* (3), 1845.
- (4) Lutz, T. A. J. A. Creating the amylin story. **2022**, *172*, 105965.
- (5) Wu, Y.; Ding, Y.; Tanaka, Y.; Zhang, W. J. I. j. o. m. s. Risk factors contributing to type 2 diabetes and recent advances in the treatment and prevention. **2014**, *11* (11), 1185.
- (6) Blair, S. N. J. B. j. o. s. m. Physical inactivity: the biggest public health problem of the 21st century. **2009**, *43* (1), 1.
- (7) Horta, B. L.; Loret de Mola, C.; Victora, C. G. J. A. p. Long-term consequences of breastfeeding on cholesterol, obesity, systolic blood pressure and type 2 diabetes: a systematic review and meta-analysis. **2015**, *104*, 30.
- (8) Hillier, T. A.; Pedula, K. L. J. D. c. Characteristics of an adult population with newly diagnosed type 2 diabetes: the relation of obesity and age of onset. **2001**, *24* (9), 1522.
- (9) De Pergola, G.; Triggiani, V.; Bartolomeo, N.; Nardecchia, A.; Angelo Giagulli, V.; Bruno, I.; Caccavo, D.; Silvestris, F. J. E., Metabolic; Targets, I. D.-D. Independent relationship of osteocalcin circulating levels with obesity, type 2 diabetes, hypertension, and HDL cholesterol. **2016**, *16* (4), 270.
- (10) Jaikaran, E. T.; Clark, A. Islet amyloid and type 2 diabetes: from molecular misfolding to islet pathophysiology. *Biochimica et Biophysica Acta (BBA)-Molecular Basis of Disease* **2001**, *1537* (3), 179.
- (11) Saeedi, P.; Petersohn, I.; Salpea, P.; Malanda, B.; Karuranga, S.; Unwin, N.; Colagiuri, S.; Guariguata, L.; Motala, A. A.; Ogurtsova, K. Global and regional diabetes prevalence estimates for 2019 and projections for 2030 and 2045: Results from the International Diabetes Federation Diabetes Atlas. *Diabetes research and clinical practice* **2019**, *157*, 107843.
- (12) Zhang, M.; Hu, R.; Chen, H.; Chang, Y.; Gong, X.; Liu, F.; Zheng, J. Interfacial interaction and lateral association of cross-seeding assemblies between hIAPP and rIAPP oligomers. *Physical Chemistry Chemical Physics* **2015**, *17* (16), 10373.
- (13) Kapurniotu, A. Amyloidogenicity and cytotoxicity of islet amyloid polypeptide. *Peptide Science: Original Research on Biomolecules* **2001**, *60* (6), 438.
- (14) Patel, H. R.; Pithadia, A. S.; Brender, J. R.; Fierke, C. A.; Ramamoorthy, A. J. T. J. o. P. C. L. In search of aggregation pathways of IAPP and other amyloidogenic proteins: finding answers through NMR spectroscopy. **2014**, *5* (11), 1864.
- (15) Weyer, C.; Maggs, D. G.; Young, A. A.; Kolterman, O. G. J. C. p. d. Amylin replacement with pramlintide as an adjunct to insulin therapy in type 1 and type

- 2 diabetes mellitus: a physiological approach toward improved metabolic control. **2001**, *7* (14), 1353.
- (16) Guo, J.; Sun, W.; Li, L.; Liu, F.; Lu, W. Brazilin inhibits fibrillogenesis of human islet amyloid polypeptide, disassembles mature fibrils, and alleviates cytotoxicity. *RSC advances* **2017**, *7* (69), 43491.
- (17) Ren, B.; Liu, Y.; Zhang, Y.; Zhang, M.; Sun, Y.; Liang, G.; Xu, J.; Zheng, J. J. J. o. M. C. B. Tanshinones inhibit hIAPP aggregation, disaggregate preformed hIAPP fibrils, and protect cultured cells. **2018**, *6* (1), 56.
- (18) Zhang, Y.; Zhang, D.; Tang, Y.; Ren, B.; Liu, F.; Xu, L.; Chang, Y.; Zheng, J. J. M. A. Aromadendrin: a dual amyloid promoter to accelerate fibrillization and reduce cytotoxicity of both amyloid- $\beta$  and hIAPP. **2020**, *1* (5), 1241.
- (19) Meleleo, D.; Gerbino, A.; Mastrodonato, M. J. B. C. Evidence of the different effect of mercury and cadmium on the hIAPP aggregation process. **2022**, *290*, 106880.
- (20) Sparks, S.; Liu, G.; Robbins, K. J.; Lazo, N. D. Curcumin modulates the self-assembly of the islet amyloid polypeptide by disassembling  $\alpha$ -helix. *Biochemical and biophysical research communications* **2012**, *422* (4), 551.
- (21) Franko, A.; Rodriguez Camargo, D. C.; Böddrich, A.; Garg, D.; Rodriguez Camargo, A.; Rathkolb, B.; Janik, D.; Aichler, M.; Feuchtinger, A.; Neff, F. J. S. r. Epigallocatechin gallate (EGCG) reduces the intensity of pancreatic amyloid fibrils in human islet amyloid polypeptide (hIAPP) transgenic mice. **2018**, *8* (1), 1116.
- (22) Mishra, R.; Sellin, D.; Radovan, D.; Gohlke, A.; Winter, R. J. C. Inhibiting islet amyloid polypeptide fibril formation by the red wine compound resveratrol. **2009**, *10* (3), 445.
- (23) Tang, Y.; Zhang, D.; Zhang, Y.; Liu, Y.; Gong, X.; Chang, Y.; Ren, B.; Zheng, J. J. A. A. B. M. Introduction and fundamentals of human islet amyloid polypeptide inhibitors. **2020**, *3* (12), 8286.
- (24) Cox, S. J.; Camargo, D. C. R.; Lee, Y.-H.; Dubini, R. C.; Rovó, P.; Ivanova, M. I.; Padmini, V.; Reif, B.; Ramamoorthy, A. J. C. C. Small molecule induced toxic human-IAPP species characterized by NMR. **2020**, *56* (86), 13129.
- (25) Kusminski, C. M.; McTernan, P. G.; Kumar, S. J. C. s. Role of resistin in obesity, insulin resistance and Type II diabetes. **2005**, *109* (3), 243.
- (26) Hudish, L. I.; Reusch, J. E.; Sussel, L. J. T. J. o. c. i.  $\beta$  Cell dysfunction during progression of metabolic syndrome to type 2 diabetes. **2019**, *129* (10), 4001.
- (27) Berbudi, A.; Rahmadika, N.; Tjahjadi, A. I.; Ruslami, R. J. C. d. r. Type 2 diabetes and its impact on the immune system. **2020**, *16* (5), 442.
- (28) Oguntibeju, O. O. J. I. j. o. p., pathophysiology; pharmacology. Type 2 diabetes mellitus, oxidative stress and inflammation: examining the links. **2019**, *11* (3), 45.
- (29) Gonzalez, L. L.; Garrie, K.; Turner, M. D. J. B. e. B. A.-M. B. o. D. Type 2 diabetes—an autoinflammatory disease driven by metabolic stress. **2018**, *1864* (11), 3805.

- (30) El Saghir, A.; Farrugia, G.; Vassallo, N. J. C.; Lipids, P. o. The human islet amyloid polypeptide in protein misfolding disorders: Mechanisms of aggregation and interaction with biomembranes. **2021**, *234*, 105010.
- (31) Dupuis, N. F.; Wu, C.; Shea, J.-E.; Bowers, M. T. J. J. o. t. A. C. S. The amyloid formation mechanism in human IAPP: dimers have  $\beta$ -strand monomer–monomer interfaces. **2011**, *133* (19), 7240.
- (32) Tang, Y.; Liu, Y.; Zhang, Y.; Zhang, D.; Gong, X.; Zheng, J. J. A. C. N. Repurposing a cardiovascular disease drug of cloridarol as hIAPP inhibitor. **2021**, *12* (8), 1419.
- (33) Yang, G.; Wei, J.; Liu, P.; Zhang, Q.; Tian, Y.; Hou, G.; Meng, L.; Xin, Y.; Jiang, X. J. M. Role of the gut microbiota in type 2 diabetes and related diseases. **2021**, *117*, 154712.
- (34) Albandar, J. M.; Rams, T. E. J. P. Global epidemiology of periodontal diseases: an overview. **2002**, *29* (1), 7.
- (35) D'aiuto, F.; Sabbah, W.; Netuveli, G.; Donos, N.; Hingorani, A. D.; Deanfield, J.; Tsakos, G. J. T. J. o. C. E.; Metabolism. Association of the metabolic syndrome with severe periodontitis in a large US population-based survey. **2008**, *93* (10), 3989.
- (36) Xie, K.; Xu, B.; Zhang, Y.; Chen, M.; Ji, Y.; Wang, J.; Huang, Z.; Zhou, K.; Xia, Y.; Tang, W. J. J. o. c. p. A multi - method evaluation of the effects of Inflammatory cytokines (IL-1 $\beta$ , IFN- $\gamma$ , TNF- $\alpha$ ) on pancreatic  $\beta$ -cells. **2018**, *233* (12), 9375.
- (37) Wachlin, G.; Augstein, P.; Schröder, D.; Kuttler, B.; Klötting, I.; Heinke, P.; Schmidt, S. J. J. o. a. IL-1 $\beta$ , IFN- $\gamma$  and TNF- $\alpha$  increase vulnerability of pancreatic beta cells to autoimmune destruction. **2003**, *20* (4), 303.
- (38) Demmer, R.; Jacobs Jr, D.; Singh, R.; Zuk, A.; Rosenbaum, M.; Papapanou, P.; Desvarieux, M. J. J. o. d. r. Periodontal bacteria and prediabetes prevalence in ORIGINS: the oral infections, glucose intolerance, and insulin resistance study. **2015**, *94* (9\_suppl), 201S.
- (39) Demmer, R. T.; Breskin, A.; Rosenbaum, M.; Zuk, A.; LeDuc, C.; Leibel, R.; Paster, B.; Desvarieux, M.; Jacobs Jr, D. R.; Papapanou, P. N. J. J. o. c. p. The subgingival microbiome, systemic inflammation and insulin resistance: the oral infections, glucose intolerance and insulin resistance study. **2017**, *44* (3), 255.
- (40) Hjelmessaeth, J.; Asberg, A.; Muller, F.; Hartmann, A.; Jenssen, T. J. C. d. r. New-onset posttransplantation diabetes mellitus: insulin resistance or insulinopenia? Impact of immunosuppressive drugs, cytomegalovirus and hepatitis C virus infection. **2005**, *1* (1), 1.
- (41) Hjelmessaeth, J.; Sagedal, S.; Hartmann, A.; Rollag, H.; Egeland, T.; Hagen, M.; Nordal, K.; Jenssen, T. J. D. Asymptomatic cytomegalovirus infection is associated with increased risk of new-onset diabetes mellitus and impaired insulin release after renal transplantation. **2004**, *47*, 1550.
- (42) Westwell-Roper, C.; Dai, D. L.; Soukhatcheva, G.; Potter, K. J.; van Rooijen, N.; Ehses, J. A.; Verchere, C. B. J. T. j. o. i. IL-1 blockade attenuates islet amyloid

- polypeptide-induced proinflammatory cytokine release and pancreatic islet graft dysfunction. **2011**, *187* (5), 2755.
- (43) Masters, S. L.; Dunne, A.; Subramanian, S. L.; Hull, R. L.; Tannahill, G. M.; Sharp, F. A.; Becker, C.; Franchi, L.; Yoshihara, E.; Chen, Z. J. N. i. Activation of the NLRP3 inflammasome by islet amyloid polypeptide provides a mechanism for enhanced IL-1 $\beta$  in type 2 diabetes. **2010**, *11* (10), 897.
- (44) Farrim, M. I. d. J. D., 2021.
- (45) Wang, C.; Ma, Y.-H.; Han, X.; Lu, X. J. L. Re-Examining Interaction between Antimicrobial Peptide Aurein 1.2 and Model Cell Membranes via SFG. **2022**.
- (46) Niu, Z.; Prade, E.; Malideli, E.; Hille, K.; Jussupow, A.; Mideksa, Y. G.; Yan, L. M.; Qian, C.; Fleisch, M.; Messias, A. C. J. A. C. Structural Insight into IAPP-Derived Amyloid Inhibitors and Their Mechanism of Action. **2020**, *132* (14), 5820.
- (47) Fernandez, D. I.; Le Brun, A. P.; Whitwell, T. C.; Sani, M.-A.; James, M.; Separovic, F. J. P. C. C. P. The antimicrobial peptide aurein 1.2 disrupts model membranes via the carpet mechanism. **2012**, *14* (45), 15739.
- (48) Wang, L.; Liu, Q.; Chen, J.-C.; Cui, Y.-X.; Zhou, B.; Chen, Y.-X.; Zhao, Y.-F.; Li, Y.-M. J. B. c. Antimicrobial activity of human islet amyloid polypeptides: an insight into amyloid peptides' connection with antimicrobial peptides. **2012**, *393* (7), 641.
- (49) Zhou, K.; Wang, M.; Zhou, Y.; Sun, M.; Xie, Y.; Yu, D.-G. J. A. C.; Materials, H. Comparisons of antibacterial performances between electrospun polymer@ drug nanohybrids with drug-polymer nanocomposites. **2022**, *5* (2), 907.
- (50) Tang, Y.; Zhang, D.; Gong, X.; Zheng, J. J. B. C. A mechanistic survey of Alzheimer's disease. **2022**, *281*, 106735.
- (51) Micsonai, A.; Wien, F.; Kernya, L.; Lee, Y.-H.; Goto, Y.; Réfrégiers, M.; Kardos, J. Accurate secondary structure prediction and fold recognition for circular dichroism spectroscopy. *Proceedings of the National Academy of Sciences* **2015**, *112* (24), E3095.
- (52) Li, Z.; Narouz, M. R.; Munro, K.; Hao, B.; Crudden, C. M.; Horton, J. H.; Hao, H. Carboxymethylated dextran-modified n-heterocyclic carbene self-assembled monolayers on gold for use in surface plasmon resonance biosensing. *ACS applied materials & interfaces* **2017**, *9* (45), 39223.